Journal of Alloys and Compounds 509 (2011) 9157–9163

Contents lists available at ScienceDirect

Journal of Alloys and Compounds

journal homepage: www.elsevier.com/locate/jallcom

Synthesis, characterization and photocatalytic activity of $NaNbO_3$/ZnO heterojunction photocatalysts

Hui Xu[a,b], Chengtang Liu[a,b], Huaming Li[a,*], Yuanguo Xu[a], Jiexiang Xia[a], Sheng Yin[a], Ling Liu[a], Xiangyang Wu[b]

[a] School of Chemistry and Chemical Engineering, Jiangsu University, Zhenjiang 212013, PR China
[b] School of the Environment, Jiangsu University, Zhenjiang 212013, PR China

ARTICLE INFO

Article history:
Received 23 January 2011
Received in revised form 22 June 2011
Accepted 23 June 2011
Available online 30 June 2011

Keywords:
$NaNbO_3$/ZnO
Heterojunction
Photocatalytic
Methylene blue

ABSTRACT

A series of $NaNbO_3$/ZnO heteronanostructures were synthesized with the hydrothermal method. Various characterization methods such as X-ray powder diffraction (XRD), scanning electronic microscope (SEM) and energy dispersive X-ray spectrometer (EDS), transmission electron microscope (TEM), X-ray photoelectron spectra (XPS) and diffuse reflectance spectra (DRS) were employed to investigate the structure, morphology and photocatalytic properties. The photocatalytic activity of the catalysts was evaluated by the degradation of methylene blue dye and the highest photocatalytic efficiency was observed when the content of $NaNbO_3$ was 10 wt.%. The photocatalytic mechanism of the heterojunction was also discussed. The effective transformation of the photoexcited electron and holes restricted the recombination of charges, which was regarded as the main reason of the high photocatalytic activity.

1. Introduction

In recent years, many kinds of novel heterogeneous metal oxide semiconductor materials, such as TiO_2 [1], ZnS [2,3], ZnO and Fe_2O_3 nanocatalysts have been developed for environmental remediation [4–8]. Among various semiconductor nanostructures, ZnO, with a band gap of 3.37 eV, has attracted much attention in such fields as gas sensors [9–11], electrical and optical devices [12–14], field-emitters [15], electrostatic dissipative coating and catalysts for liquid phase hydrogenation [16,17]. Besides, it is an effective catalyst which can degrade various organic pollutants under UV (ultraviolet) irradiation [18–22]. So far, a variety of nanostructures of ZnO has been investigated: nanowires and nanorods, nano-flowers, nanoribbons, nanonails, nanopencils and nanoparticles [23–26]. Most of them can be prepared with various methods such as thermal evaporation, cyclic feeding chemical vapor deposition [27], chemical vapor deposition [28], wet chemical reactions, electrochemical techniques, sol–gel technique, hydrothermal method, etc. However, the photocatalytic ability of the sample is not high enough.

Photocatalytic oxidation involves the adsorption of the pollutant on the surface and the oxidation on the catalyst surface or in its vicinity [29]. In the oxidation process, photocatalytic oxidation of organic pollutants is based on the electron–hole pair. However, the high recombination rate of the photogenerated electron–hole pairs hinders the practical application [30]. Therefore, it is essential to prohibit the recombination of photogenerated electron–hole pairs in the semiconductors to achieve the high photocatalytic activity [31]. A lot of efforts have been made to improve the photocatalytic activity of semiconductors, such as metals doping, semiconductor combination and co-doping techniques [32–34]. Among these methods, semiconductor-based heterostructure has received much attention recently because it can present excellent separation rate when separating photo-induced electron and holes [35]. Therefore, many heterostructured photocatalysts with high photocatalytic activity have been investigated, such as ZnO/SnO [36], Bi_2O_3/$BaTiO_3$ [37], BiOI/TiO_2 [38], graphene oxide/TiO_2 [39].

It has been reported that sodium niobate can be used as an effective photocatalyst [40–42]. From the above analysis, it can be inferred that the $NaNbO_3$/ZnO structure would increase the photocatalytic activity. To the best of our knowledge, there is seldom research on the synthesis and photocatalysis of $NaNbO_3$/ZnO heterojunction catalysts. In this present work, $NaNbO_3$/ZnO heterostructured photocatalyst was successfully prepared with the hydrothermal method. During the degradation process of methylene blue (MB) under UV light irradiation, the $NaNbO_3$/ZnO heterostructure showed much higher photocatalytic activity than ZnO, while $NaNbO_3$/ZnO (10 wt.%) possessed the highest activity. The structure of the heterojunction was characterized by X-ray diffraction (XRD), scanning electron microscopy combined

* Corresponding author. Tel.: +86 511 88791800; fax: +86 511 88791708.
E-mail address: lihm@ujs.edu.cn (H. Li).

0925-8388/$ – see front matter © 2011 Elsevier B.V. All rights reserved.
doi:10.1016/j.jallcom.2011.06.100

with energy-dispersive X-ray spectroscopy (SEM-EDS), transmission electron microscope (TEM), X-ray photoelectron spectroscopy (XPS) and diffuse reflectance spectroscopy (DRS). The possible photocatalytic mechanism of the $NaNbO_3$/ZnO catalysts was also studied.

2. Experimental

2.1. Preparation of ZnO and $NaNbO_3$/ZnO heterojunction nanocatalyst

ZnO was prepared by a simple hydrothermal reaction, with 3 mmol zinc acetate and 3.6 mmol NaOH dissolving into 20 ml of distilled H_2O. After being stirred for 20 min at room temperature, the reaction mixtures were transferred into a 25 ml Teflon-lined stainless steel autoclave, which was then sealed and heated in an oven up to 180 °C. Such temperature was maintained for 24 h. When the reaction finished, the autoclave was cooled down to room temperature naturally. After being cooled down, the resultant precipitate was centrifuged and washed with distilled water and absolute ethanol. At last, the obtained product was dried at 60 °C.

The $NaNbO_3$/ZnO heterojunction nanocatalyst was also synthesized using the hydrothermal method. The procedures are as follows: a certain amount of Nb_2O_5, zinc acetate and NaOH were dissolved into 20 ml of deionized water at room temperature with agitation for 30 min. The resultant sol was poured into a 25 ml Teflon-lined stainless steel autoclave, which was then sealed and kept at 180 °C for 24 h. The resultant precipitate was treated the same as the above.

2.2. Catalysts characterization

The crystal structures of the synthesized powders were determined by X-ray powder diffraction (XRD) on a Bruker D8 diffractometer with Cu Kα radiation (λ = 1.5418 Å) in the range of 2θ = 10–80°. The nanoparticle morphology was measured using a scanning electronic microscope (SEM, JEOL JSM-7001F) and a transmission electron microscope (TEM, H-600-II, Hitachi). The chemical compositions of the catalysts were determined using energy dispersive X-ray spectrometer (EDS) attached to the SEM. The diffuse reflectance spectra (DRS) were collected using UV–vis spectrometer (UV-2450, Shimadzu) in the range of 240–800 nm. $BaSO_4$ was used as the reflectance standard material. X-ray photoelectron spectra (XPS) measurements of synthesized $NaNbO_3$/ZnO nanoparticles were carried out on an ESCALab MKII X-ray photo-electron spectrometer using the Mg Kα radiation at room temperature.

2.3. Evaluation of catalytic activity: degradation of MB

The catalytic activity of the catalysts was evaluated by degradation of MB dye. 0.1 g sample was put into 100 ml MB dye solution with a concentration of 10 mg l^{-1}. The photocatalytic reactor consists of a quartz glass with a circulating water jack and two mercury lamps (125 W × 2). The slurry was first magnetically stirred for 30 min to ensure the adsorption/desorption equilibrium. During the reaction, 5 ml suspension was taken from the Pyrex reaction glass and separated through centrifugation. The catalytic degradation efficiency (E) of MB was obtained by the following formula:

$$E = \frac{C_0 - C}{C_0} \times 100\% = \frac{A_0 - A}{A_0} \times 100\% \quad (1)$$

where C is the concentration of the MB solution at the reaction time t, C_0 is the adsorption/desorption equilibrium concentration of MB (at reaction time 0); A and A_0 are the corresponding values which are determined by measuring the absorbance at 664 nm with UV–vis spectrometry.

3. Results and discussion

3.1. XRD analysis

Fig. 1 shows the XRD patterns of $NaNbO_3$/ZnO catalysts with different $NaNbO_3$ contents. In Fig. 1, the peaks at 2θ = 31.8°, 34.4°, 36.3°, 47.5°, 56.6°, 62.9°, 66.4°, 68.0°, 69.1°, 72.6° and 77.0° were assigned to the (100), (002), (101), (102), (110), (103), (200), (112), (201), (004) and (202) planes of the ZnO phase respectively (JCPDS no. 36-1451), which were marked with "*". In Fig. 1(a–g) it was found that with the increasing content of $NaNbO_3$, the characteristic peaks at 22.9°, 32.5°, 46.3°, 52.6°, 57.9°, 68.2° appeared, which was identical with the $NaNbO_3$ standard card (JCPDS no. 33-1270). It could be seen that no extra peaks except for $NaNbO_3$ and ZnO were detected in XRD analysis, which suggested that the compositions of the above sample were ZnO and $NaNbO_3$. With the increasing Nb content, the diffraction peaks of $NaNbO_3$ were strengthened gradually, as seen in Fig. 1(a–g).

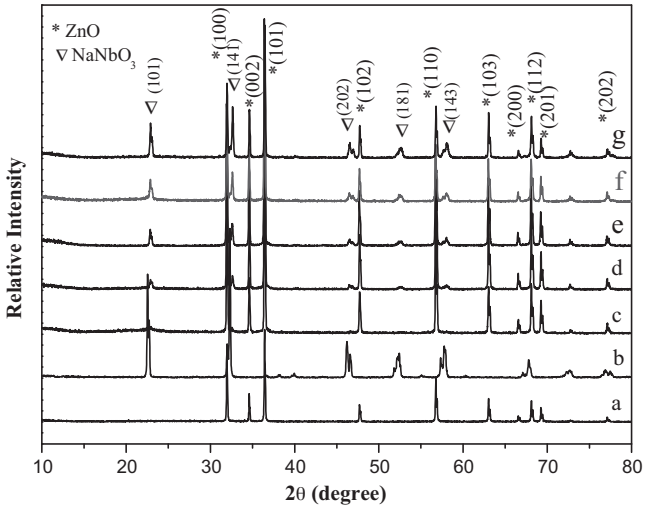

Fig. 1. XRD patterns of $NaNbO_3$/ZnO catalysts synthesized at 180 °C with different $NaNbO_3$ contents: (a) 0, (b) 100 wt.%, (c) 2 wt.%, (d) 5 wt.%, (e) 10 wt.%, (f) 20 wt.% and (g) 40 wt.%.

3.2. SEM-EDS analysis

Fig. 2 shows the SEM images of pure ZnO, pure $NaNbO_3$ and $NaNbO_3$/ZnO composites. The images revealed that pure ZnO sample was composed of small nanorod in wild disorder, and the length of the sample was in the range of 100 nm to 1 μm (Fig. 2(a)). However, the morphology of the pure $NaNbO_3$ was quite different from that of the pure ZnO sample. As shown in Fig. 2(b), the pure $NaNbO_3$ was cube, and the width was 0.5–2 μm. Both the cube and nanorod morphology could be seen in Fig. 2(c and d). The EDS spectral made it clear that the sample was composed of Na, Nb, Zn and O (Fig. 2(e)) which was in accord with the XRD result.

3.3. XPS analysis

The surface chemical states of the element were characterized by XPS measurements. The overall XPS spectra of $NaNbO_3$/ZnO composite powders are shown in Fig. 3. All the binding energy (BE) values were referred to the C 1s photoemission line at 284.5 eV. The high-resolution spectra of $NaNbO_3$/ZnO composites were shown in Fig. 4. It could be seen the Nb 3d spectra consisted of two peaks at 210.0 eV and 207.2 eV corresponding to their angular momentum of electrons (Fig. 4(a)). The Na 1s orbital showed peaks at 1071.9 eV (Fig. 4(b)). The peak centered at 1021.9 eV was in accord with that of the Zn 2p3/2 (Fig. 4(c)), which was consistent with the literature [43]. From these results, it could be confirmed that the $NaNbO_3$/ZnO catalysts consisted of ZnO and $NaNbO_3$.

3.4. Diffuse reflection spectra analysis

Fig. 5(a) shows DRS of ZnO, $NaNbO_3$ and $NaNbO_3$/ZnO (10 wt.%) samples. Compared with the pure ZnO, the $NaNbO_3$/ZnO sample showed a little stronger absorbance in the wavelength range of 200–400 nm. The curve shape of the DRS spectrum of $NaNbO_3$/ZnO sample hardly changed with $NaNbO_3$ added. These demonstrated that the modified $NaNbO_3$ did not give rise to new spectrum phenomena. It was also found that the absorption band of the samples were all below 400 nm, which indicated the ZnO, $NaNbO_3$ and $NaNbO_3$/ZnO samples could only be induced by UV light.

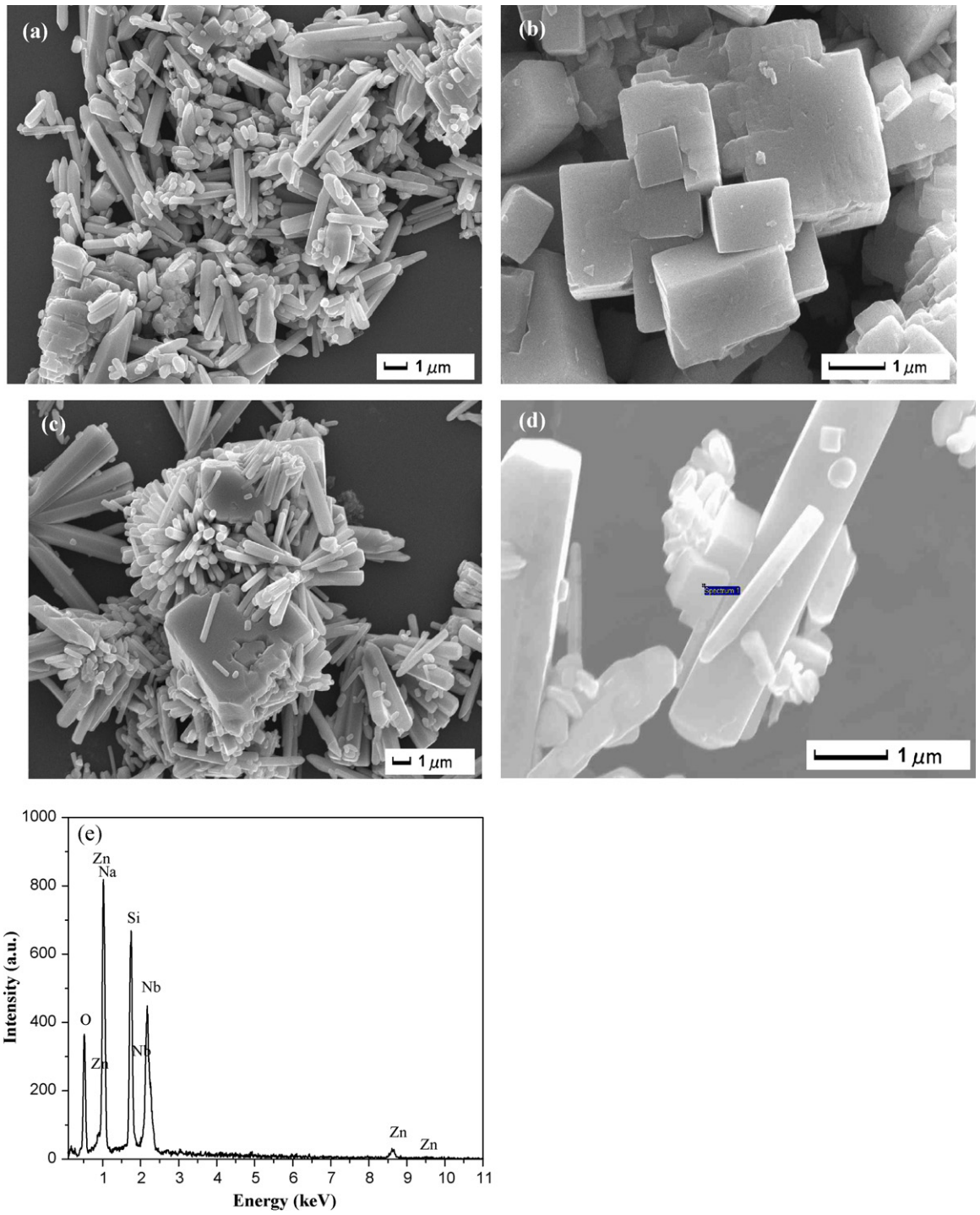

Fig. 2. SEM images of: (a) pure ZnO, (b) pure $NaNbO_3$, (c and d) $NaNbO_3$/ZnO (10 wt.%), (e) EDS spectrum of the cube structure in $NaNbO_3$/ZnO (10 wt.%).

The estimated value of the band gap (E_g) of the samples could be calculated using the following equation:

$$A = \frac{C(h\nu - E_g)^{1/2}}{h\nu} \quad (2)$$

where A, ν, E_g, and C are the absorption coefficient, the light frequency, the band gap, and a constant, respectively. The estimated band gap energies for ZnO, $NaNbO_3$/ZnO (10 wt.%) and $NaNbO_3$ samples were 3.37 eV, 3.33 eV and 3.30 eV respectively (Fig. 5(b)).

3.5. Photocatalytic degradation of MB

To evaluate the photocatalytic activity of the prepared $NaNbO_3$/ZnO samples, experiments were carried out by decomposing MB solution. Fig. 6 showed the effect of different contents of $NaNbO_3$ on the photocatalytic activity of $NaNbO_3$/ZnO composites under UV light irradiation. In Fig. 6, the photocatalytic activity of $NaNbO_3$/ZnO composites was higher than that of the pure ZnO catalyst. It was observed that the photocatalytic efficiency increased with $NaNbO_3$ loading up to 10 wt.%. Increasing the $NaNbO_3$ content continuously could decrease the photocatalytic

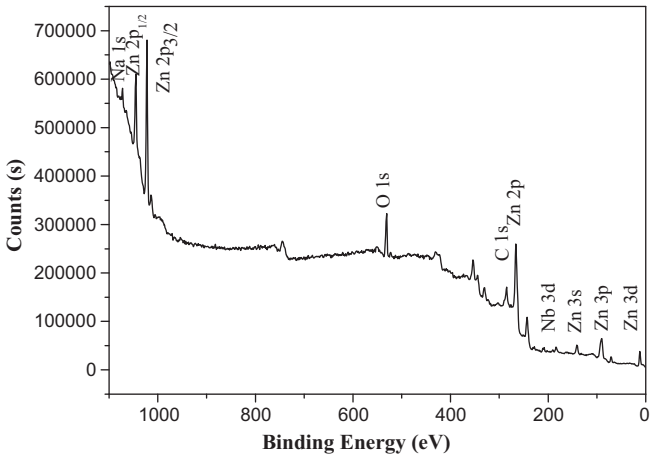

Fig. 3. XPS spectra of $NaNbO_3$/ZnO (10 wt.%) composite photocatalysts.

activity. The photocatalytic activity followed the increasing order of 0 wt.% < 40 wt.% < 20 wt.% < 5 wt.% < 10 wt.%. The 10 wt.% $NaNbO_3$/ZnO nanocomposites showed the highest catalytic efficiency: ca. 97% of the MB was degraded in 1 h irradiation. By considering that only 70% and 80% of the MB was degraded by TiO_2 (Degussa P25) and the pure ZnO system respectively, the decomposition efficiency achieved by $NaNbO_3$/ZnO sample was quite remarkable. It was found that other organic dyes such as methyl orange (MO) and Rhodamine B (RhB) were also degraded by $NaNbO_3$/ZnO (10 wt.%) photocatalysts. However, the photocatalytic degradation efficiency of MO and RhB was 40% and 51% in 1 h irradiation respectively.

3.6. Kinetics

To investigate the kinetics of MB degradation over the $NaNbO_3$/ZnO catalysts, a pseudo first-order reaction model was introduced to describe the experimental data as follows:

$$-\ln\left(\frac{C}{C_0}\right) = k_{ap}t \quad (3)$$

where k_{ap} is the apparent rate constant, C_0 is the initial concentration of MB, t is the reaction time and C is the concentration of MB at the reaction time of t. Fig. 7 shows the kinetic fit for the decomposition of MB over $NaNbO_3$/ZnO catalysts under UV irradiation. The correlation coefficient values (R) listed in the inset table of Fig. 7 were all higher than 0.99. It appeared that all of them followed the first-order reaction kinetics. The apparent rate constant (k) of the pure ZnO was found to be 0.01513 min^{-1}. After introduction of $NaNbO_3$ (from 5 to 40 wt.%), the reaction rate constants (k) were 0.02191, 0.02888, 0.0184 and 0.01578 min^{-1} under UV light irradiation. It was interesting to note that the maximum value was 1.9 times as large as that of the pure ZnO.

Moreover, Fig. 8 showed the photocatalytic degradation of MB over $NaNbO_3$/ZnO (10 wt.%) photocatalysts under UV light irradiation with three-times cycle use. It was indicated that the

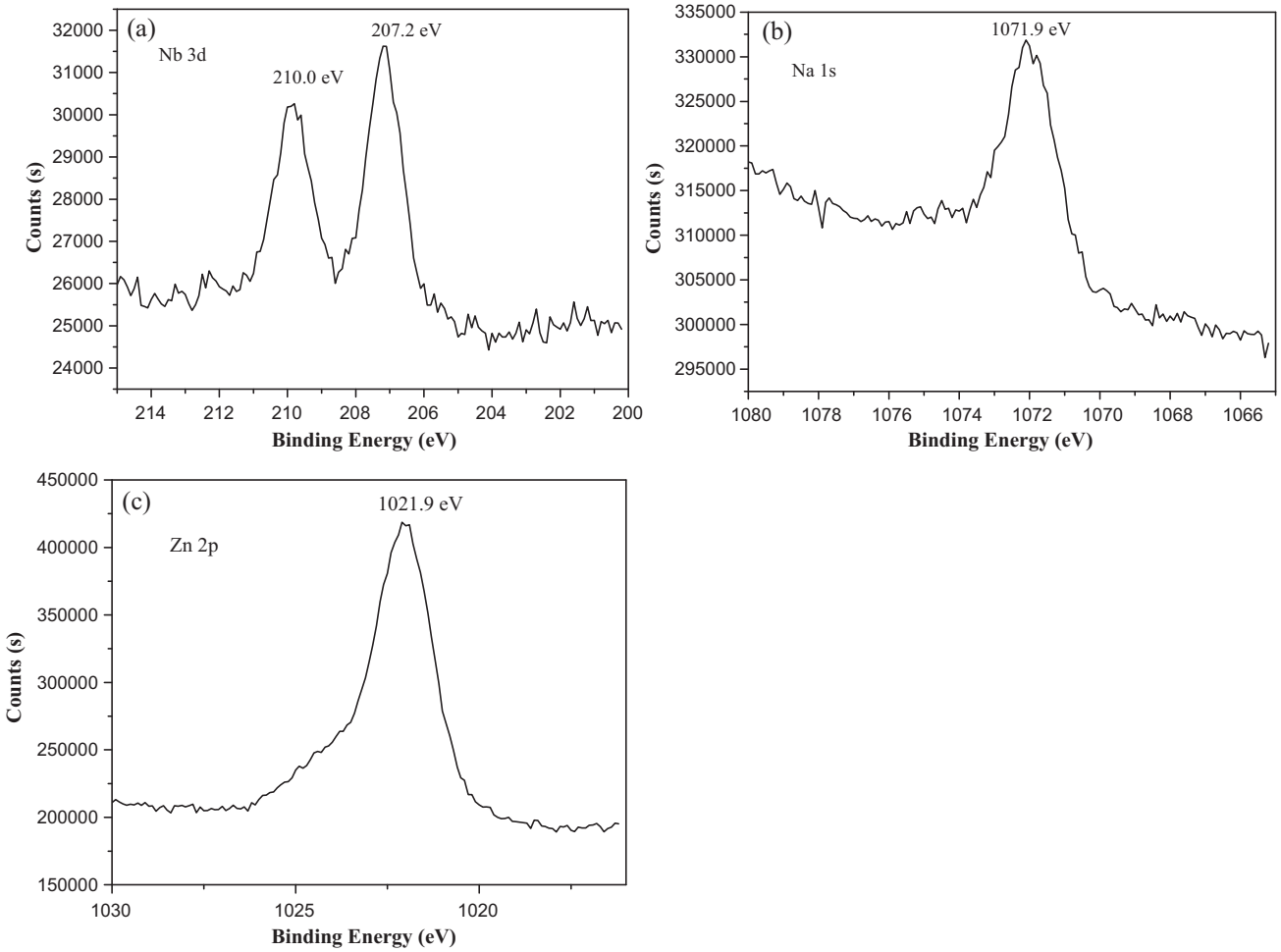

Fig. 4. High-resolution XPS spectra of $NaNbO_3$/ZnO: (a) Nb 3d, (b) Na 1 s and (c) Zn 2p.

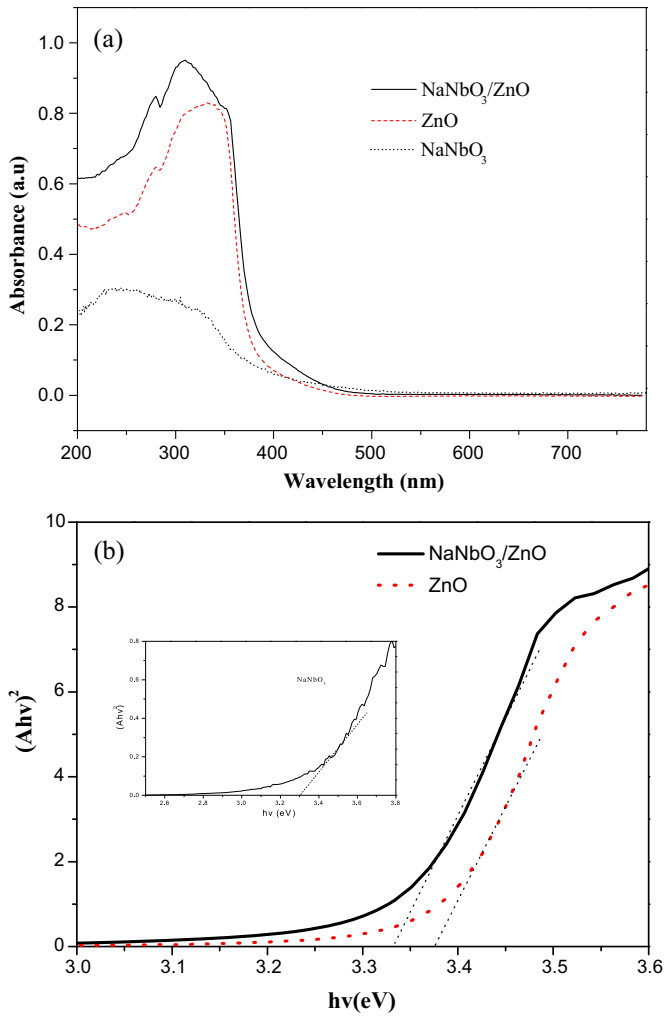

Fig. 5. DRS (a) of ZnO, $NaNbO_3$ and $NaNbO_3$/ZnO (10 wt.%) samples; (b) estimated band gap of ZnO, $NaNbO_3$ and $NaNbO_3$/ZnO (10 wt.%).

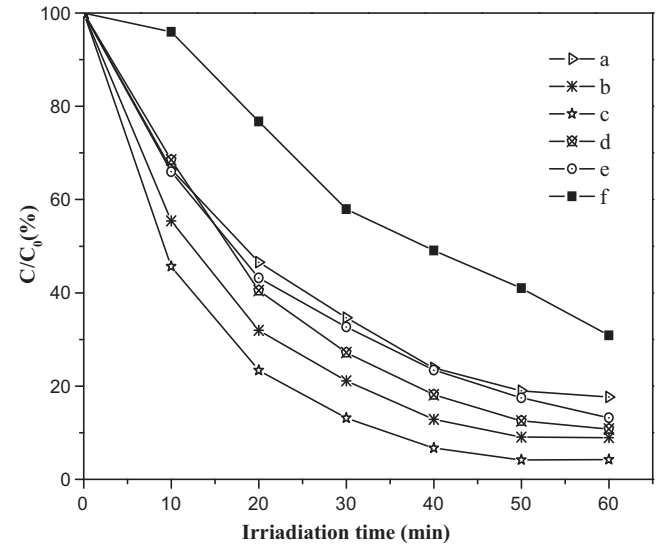

Fig. 6. Photocatalytic activities of: (a) pure ZnO, $NaNbO_3$/ZnO composites with different $NaNbO_3$ contents under UV light irradiation: (b) 5 wt.%, (c) 10 wt.%, (d) 20 wt.%, (e) 40 wt.% and (f) P25-TiO_2.

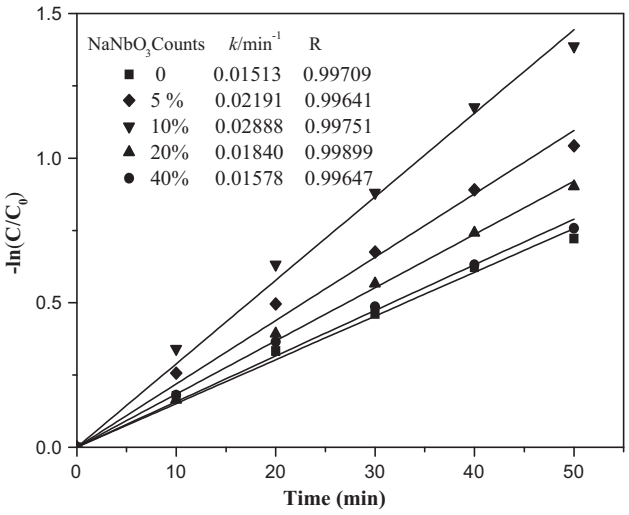

Fig. 7. Influence of different $NaNbO_3$ contents on the degradation kinetics of MB under UV light irradiation.

$NaNbO_3$/ZnO composite was stable under repeated use, which suggested its potential industrial application.

3.7. Absorption spectral changes during the photocatalytic degradation of MB by photocatalysts

The temporal evolution of the absorption spectral changes during the photocatalytic degradation of MB over ZnO and $NaNbO_3$/ZnO (10 wt.%) catalysts under UV light irradiation is shown in Fig. 9. It could be seen that the MB was sharply degraded in the case of $NaNbO_3$/ZnO (10 wt.%) composites. The main absorption band at 664 nm almost completely disappeared after 1 h under UV light irradiation in the presence of $NaNbO_3$/ZnO composites (Fig. 9(b)). Meanwhile, the color of the suspension changed gradually, which indicated the chromophoric structure of the MB dye was decomposed.

3.8. Photocatalytic mechanism

The role of $NaNbO_3$ in $NaNbO_3$/ZnO composites can be analyzed as follows. The band gap of $NaNbO_3$ was estimated as 3.3 eV according to the DRS analysis (Fig. 5(b)), and it was a p-type

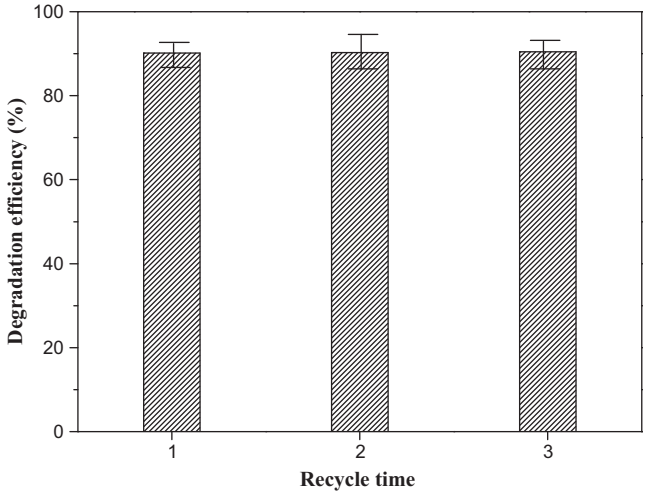

Fig. 8. Photocatalytic activity of the $NaNbO_3$/ZnO (10 wt.%) photocatalysts for MB degradation with three-times cycle uses.

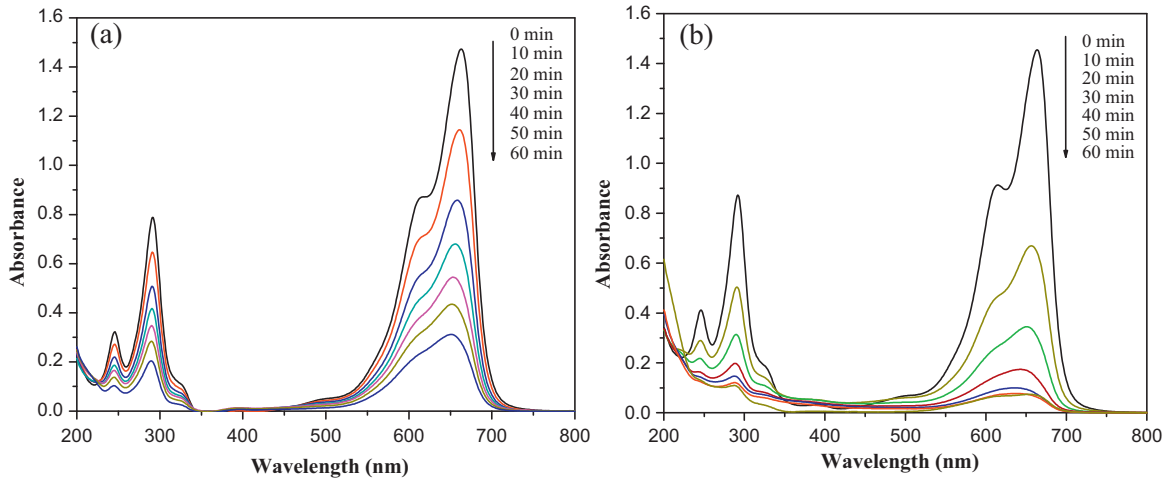

Fig. 9. Temporal UV–vis absorption spectral changes during the photocatalytic degradation of MB by (a) ZnO and (b) $NaNbO_3$/ZnO (10 wt.%) under UV light irradiation.

semiconductor compared with n-type ZnO [44,45]. So at the interface of $NaNbO_3$/ZnO composite, a p–n heterojunction would be formed. The $NaNbO_3$ cube and ZnO nanorod were composited, which could be seen by the SEM images (Fig. 2) and TEM images (Fig. 10(a and b)). The band-edge potential position of ZnO and $NaNbO_3$ played an important role in studying the flowchart of photo-excited charge carriers. To give a direct analysis, the conduction band-edge of ZnO and $NaNbO_3$ could be also estimated at the point of zero charge by the following equation:

$$E_{CB} = X - E_c - \frac{1}{2}E_g \quad (4)$$

where X is the absolute electronegativity of the atoms semiconductor, expressed as the geometric mean of the absolute electronegativity of the constituent atoms, which is defined as the arithmetic mean of the atomic electro affinity and the first ionizaion energy; E_c is the energy of free electrons of the hydrogen scale (4.5 eV); E_g is the band gap of the semiconductor. Therefore, E_c of ZnO and $NaNbO_3$ could be calculated as −0.69 eV and −0.80 eV. It indicated that the conduction band bottom of $NaNbO_3$ was more positive than that of ZnO. At the thermodynamic equilibrium of p–n heterojunction semiconductors, there was an internal field formed with the direction from n-type semiconductor to p-type semiconductor [46]. Fig. 10(c) shows the schematic diagram of the band gap structure for p–n heterojunction semiconductors formed by $NaNbO_3$ and ZnO. According to the position of band energy (Fig. 10(c)), under the UV light irradiation, the electrons in the valence band (VB) of ZnO were excited to their conduction band and left holes in VB. The holes in the VB of ZnO could transfer to the VB of $NaNbO_3$ through the interface between ZnO crystallites and $NaNbO_3$ crystallites. Besides, the electrons were injected into ZnO nanoparticles quickly since the conduction band of $NaNbO_3$ became more negative than that of ZnO. Moreover, the formed nanostructure heterojunction on $NaNbO_3$/ZnO composite also led to a more efficient interelectron transfer between the two components. Therefore, the excited electrons and holes on the semiconductors were separated and the recombination of excited electrons–holes pairs was restrained, which greatly promoted and enhanced the photocatalytic activity. Therefore, this case was favorable for photocatalysis.

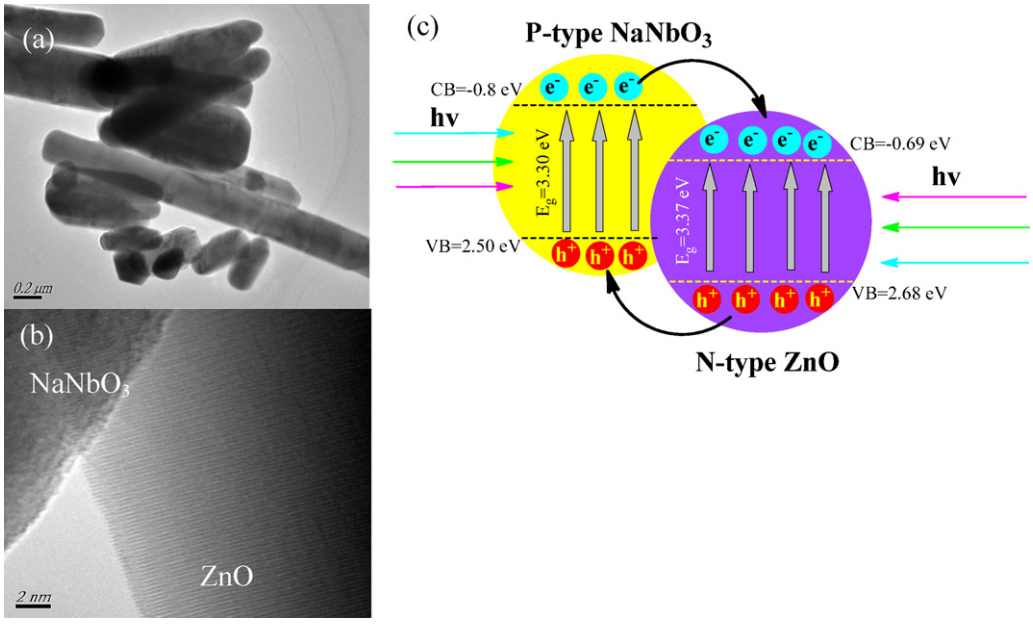

Fig. 10. The TEM image, HRTEM image and the band structure diagram of $NaNbO_3$/ZnO composite: (a) TEM image; (b) HRTEM image; (c) schematic diagram of structure of band energy for p–n heterojunction semiconductors.

4. Conclusions

In this work, the $NaNbO_3$/ZnO composites were synthesized through the hydrothermal process. The photocatalytic experiments indicated that the $NaNbO_3$/ZnO sample had much higher photocatalytic activity than ZnO because of degradation of MB under UV light. The $NaNbO_3$/ZnO (10 wt.%) sample exhibited the best photocatalytic degradation activity. The characterization results demonstrated that formation of heterojunction could accelerate the transfer of photoexcited electron and holes and thus their recombination could be restricted, which accelerated the photocatalytic activity.

Acknowledgments

The authors genuinely appreciate the financial support of this work from the National Nature Science Foundation of China (Nos. 21007021 and 21076099), Postdoctoral Foundation of China (20110490786), Research Foundation of Jiangsu University (10JDG128), Society Development Fund of Zhenjiang (SH2010006) and Doctoral Innovation Fund of Jiangsu (CX10B-275Z).

References

[1] A. Wolcott, W.A. Smith, T.R. Kuykendall, Y.P. Zhao, J.Z. Zhang, Small 5 (2009) 104–111.
[2] X.S. Fang, T.Y. Zhai, U.K. Gautam, L. Li, L.M. Wu, Y. Bando, D. Golberg, Prog. Mater. Sci. 56 (2011) 175–287.
[3] X.S. Fang, Y. Bando, U.K. Gautam, T.Y. Zhai, H.B. Zeng, X.J. Xu, M.Y. Liao, D. Golberg, Crit. Rev. Solid State Mater. Sci. 34 (2009) 190–223.
[4] R.M. Mohamed, M.A. Al-Rayyani, E.S. Baeissa, I.A. Mkhalid, J. Alloys Compd. 509 (2011) 6824–6828.
[5] M.Y. Guo, M.K. Fung, F. Fang, X.Y. Chen, A.M.C. Ng, A.B. Djurisic, W.K. Chan, J. Alloys Compd. 509 (2011) 1328–1332.
[6] J. Gupta, K.C. Barick, D. Bahadur, J. Alloys Compd. 509 (2011) 6725–6730.
[7] J. Kang, Q. Kuang, Z.X. Xie, L.S. Zheng, J. Phys. Chem. C 115 (2011) 7874–7879.
[8] Z. Zhang, C. Shao, X. Li, L. Zhang, H. Xue, C. Wang, Y. Liu, J. Phys. Chem. C 114 (2010) 7920–7925.
[9] P. Ma, Y. Wu, Z. Fu, W. Wang, J. Alloys Compd. 509 (2011) 3576–3581.
[10] R. Wahab, S.G. Ansari, Y.S. Kim, H.K. Seo, G.S. Kim, G. Khang, H.S. Shin, Mater. Res. Bull. 42 (2007) 1640–1648.
[11] Z.S. Wang, C.H. Huang, Y.Y. Huang, Y.J. Hou, P.H. Xie, B.W. Zhang, H.M. Cheng, Chem. Mater. 13 (2001) 678–682.
[12] C. Feldmann, Adv. Funct. Mater. 13 (2003) 101–107.
[13] M.J. Zheng, L.D. Zhang, G.H. Li, W.Z. Shen, Chem. Phys. Lett. 363 (2002) 123–128.
[14] R. Wu, C. Xie, Mater. Res. Bull. 39 (2004) 637–645.
[15] X.S. Fang, Y. Bando, U.K. Gautam, C. Ye, D. Golberg, J. Mater. Chem. 18 (2008) 509–522.
[16] G.M. Hamminga, G. Mul, J.A. Moulijn, Chem. Eng. Sci. 59 (2004) 5479–5485.
[17] C.A.K. Gouvea, F. Wypych, S.G. Moraes, N. Duran, N. Nagata, P. Peralta-Zamora, Chemosphere 40 (2000) 433–440.
[18] X.S. Fang, L.D. Zhang, J. Mater. Sci. Technol. 22 (2006) 1–18.
[19] M.Y. Guo, A.M.C. Ng, F.Z. Liu, A.B. Djurisic, W.K. Chan, H.M. Su, K.S. Wong, J. Phys. Chem. C 115 (2011) 11095–11101.
[20] J.J. Feng, Q.C. Liao, A.J. Wang, J.R. Chen, Cryst. Eng. Commun. 13 (2011) 4202–4210.
[21] R.M. Trommer, A.K. Alves, C.P. Bergmann, J. Alloys Compd. 491 (2010) 296–300.
[22] R. Wahab, I.H. Hwang, Y.S. Kim, H.S. Shin, Chem. Eng. J. 168 (2011) 359–366.
[23] Q.P. Luo, B.X. Lei, X.Y. Yu, D.B. Kuang, C.Y. Su, J. Mater. Chem. 21 (2011) 8709–8714.
[24] L. Feng, A. Liu, M. Liu, Y. Ma, J. Wei, B. Man, J. Alloys Compd. 492 (2010) 427–432.
[25] C.H. Ye, X.S. Fang, Y.F. Hao, X.M. Teng, L.D. Zhang, J. Phys. Chem. B 109 (2005) 19758–19765.
[26] G.Z. Shen, Y. Bando, B.D. Liu, D. Golberg, C.J. Lee, Adv. Funct. Mater. 16 (2006) 410–416.
[27] A. Umar, S. Lee, Y.S. Lee, K.S. Nahm, Y.B. Hahn, J. Cryst. Growth 277 (2005) 479–484.
[28] C.L. Wu, L. Chang, H.G. Chen, C.W. Lin, T.F. Chang, Y.C. Chao, J.K. Yan, Thin Solid Films 498 (2006) 137–141.
[29] L. Gomathi Devi, G. Krishnamurthy, J. Hazard. Mater. 162 (2009) 899–905.
[30] C.M. Teh, A.R. Mohamed, J. Alloys Compd. 509 (2011) 1648–1660.
[31] L. Zheng, Y. Zheng, C. Chen, Y. Zhan, X. Lin, Q. Zheng, K. Wei, J. Zhu, Inorg. Chem. 48 (2009) 1819–1825.
[32] Y. Xu, H. Xu, H. Li, J. Xia, C. Liu, L. Liu, J. Alloys Compd. 509 (2011) 3286–3292.
[33] J. Cui, U.J. Gibson, J. Phys. Chem. C 114 (2010) 6408–6412.
[34] G. Liu, G. Li, X. Qiu, L. Li, J. Alloys Compd. 481 (2009) 492–497.
[35] H.M. Shu, H. Xu, H.M. Li, Y.G. Xu, Z. Gu, J. Inorg. Mater. 25 (2010) 935–941.
[36] R. Liu, Y. Huang, A. Xiao, H. Liu, J. Alloys Compd. 503 (2010) 103–110.
[37] X. Lin, J. Xing, W. Wang, Z. Shan, F. Xu, F. Huang, J. Phys. Chem. C 111 (2007) 18288–18293.
[38] X. Zhang, L. Zhang, T. Xie, D. Wang, J. Phys. Chem. C 113 (2009) 7371–7378.
[39] C. Chen, W. Cai, M. Long, B. Zhou, Y. Wu, D. Wu, Y. Feng, ACS Nano 4 (2010) 6425–6432.
[40] K. Katsumata, C.E.J. Cordonier, T. Shichi, A. Fujishima, J. Am. Chem. Soc. 131 (2009) 3856–3857.
[41] G.Q. Li, N. Yang, W.L. Wang, W.F. Zhang, J. Phys. Chem. C 113 (2009) 14829–14833.
[42] J. Lv, T. Kako, Z. Li, Z. Zou, J. Ye, J. Phys. Chem. C 114 (2010) 6157–6162.
[43] S. Bai, L. Chen, D. Li, W. Yang, P. Yang, Z. Liu, A. Chen, C.L. Chung, Sens. Actuators B 146 (2010) 129–137.
[44] H. Zhu, C.X. Shan, B. Yao, B.H. Li, J.Y. Zhang, D.X. Zhao, D.Z. Shen, X.W. Fan, J. Phys. Chem. C 112 (2008) 20546–20548.
[45] Z. Guo, D. Zhao, Y. Liu, D. Shen, B. Yao, Z. Zhang, B. Li, Z. Guo, Y. Liu, J. Phys. Chem. C 114 (2010) 15499–15503.
[46] H. Jiang, H. Endo, H. Natori, M. Nagai, K. Kobayashi, Mater. Res. Bull. 44 (2009) 700–706.